

# Momentum dependence of light nuclei production in $p$ - $p$ , $p$ -Pb, and Pb-Pb collisions at energies available at the CERN Large Hadron Collider

Rui-Qin Wang,<sup>1</sup> Feng-Lan Shao<sup>1,\*</sup> and Jun Song<sup>2,†</sup>

<sup>1</sup>*School of Physics and Physical Engineering, Qufu Normal University, Shandong 273165, China*

<sup>2</sup>*Department of Physics, Jining University, Shandong 273155, China*



(Received 14 April 2021; accepted 7 June 2021; published 17 June 2021)

We study the momentum dependence of the production of light nuclei in high-energy collisions in the nucleon coalescence mechanism. We derive formulas of the momentum distributions of deuterons  $d$  and helions  ${}^3\text{He}$ . We obtain the analytic expressions of the coalescence factor  $B_A$  ( $B_2$  for  $d$  and  $B_3$  for  ${}^3\text{He}$ ) as functions of the collision system size and the momentum. We apply the deduced results to  $p$ - $p$ ,  $p$ -Pb and Pb-Pb collisions to explain naturally the interesting behavior of  $B_A$  observed in experiments at the CERN Large Hadron Collider.

DOI: [10.1103/PhysRevC.103.064908](https://doi.org/10.1103/PhysRevC.103.064908)

## I. INTRODUCTION

Light nuclei and antinuclei have provided a different window, compared with the electromagnetic and hadronic probes, to study a series of fundamental problems in high-energy physics [1–10]. The study of the production of light (anti)nuclei has attracted much attention in relativistic heavy-ion collisions recently because they are considered to be effective tools to probe the properties of the deconfined quark gluon plasma and the quantum chromodynamics phase diagram [5–7,9,10]. Two kinds of phenomenological models have proved to be particularly successful in describing the production of light nuclei. One kind is specific models based on the coalescence mechanism [11–25], and the other is statistical models [26–31]. Transport models such as those in Refs. [32–36] have also been used to describe different production characteristics of light nuclei.

Experimental data on light nuclei production accumulated recently at the BNL Relativistic Heavy Ion Collider (RHIC) and the CERN Large Hadron Collider (LHC) exhibit a number of fascinating features [37–51]. The most striking ones might be the behavior of the coalescence factor  $B_A$  as a function of the size of the collision system and the transverse momentum per nucleon  $p_T/A$  [40–42,45–51]. The coalescence factor  $B_A$  is defined as

$$E_A \frac{d^3 N_A}{d p_A^3} = B_A \left( E_p \frac{d^3 N_p}{d p_p^3} \right)^Z \left( E_n \frac{d^3 N_n}{d p_n^3} \right)^{A-Z}, \quad (1)$$

where  $E_A d^3 N_A / d p_A^3$  is the Lorentz-invariant momentum distribution of the light nuclei with mass number  $A$  and charge  $Z$ , and  $E_{p,n} d^3 N_{p,n} / d p_{p,n}^3$  are those of protons and neutrons at momentum  $p_{p,n} = p_A/A$ .

From the viewpoint of the coalescence mechanism,  $B_A$  is a unique link between the light nuclei formed and the primordial nucleons. It carries the key kinetic and dynamical information of the process of nucleons coalescing into light nuclei. Moreover,  $B_A$  can probe the freeze-out properties of the system such as the effective freeze-out volume [20,52] and freeze-out particle correlations [25] because nucleons recombining into light nuclei is expected to happen at a later stage of the system evolution [3]. Much effort has been put into the coalescence factor  $B_A$  in different coalescence models [20–25,53,54].

In the year 2020, the ALICE Collaboration published more precise data on  $B_A$  as a function of  $p_T/A$  for both  $p$ - $p$  and  $p$ -Pb collisions in separate intervals of multiplicity, which show nearly constant behavior [48,49,51]. In Pb-Pb collisions, an obvious increasing trend is observed for  $B_A$  as a function of  $p_T/A$  [46], which is usually attributed to the position-momentum correlations or hard scatterings [21,23]. A consistent and quantitative explanation for the different behavior of the  $p_T$  dependence of  $B_A$  measured in different collision systems at the LHC is urgently necessary.

In this article, we apply the coalescence mechanism to hadronic systems created in  $p$ - $p$ ,  $p$ -nucleus ( $p$ - $A$ ) and nucleus-nucleus ( $A$ - $A$ ) collisions with extremely high collision energies to study the momentum dependence of light nuclei production in the low- and intermediate- $p_T$  regions. We present simple formulas of momentum spectra and analytic expressions for momentum dependencies of  $B_A$  of different light nuclei. We find that instantaneous coalescence or recombination occurring in the nucleon rest frame rather than in the laboratory frame can give natural explanations for the obvious growth of  $B_A$  against  $p_T$  for all centralities in Pb-Pb collisions and for the relatively weak  $p_T$  dependence of  $B_A$  in  $p$ - $p$  and  $p$ -Pb collisions at the LHC [46–51].

\*shaofl@mail.sdu.edu.cn

†songjun2011@jnxu.edu.cn

Published by the American Physical Society under the terms of the [Creative Commons Attribution 4.0 International](https://creativecommons.org/licenses/by/4.0/) license. Further distribution of this work must maintain attribution to the author(s) and the published article's title, journal citation, and DOI. Funded by SCOAP<sup>3</sup>.

The rest of the paper is organized as follows: In Sec. II, we present the derivation of the momentum dependence of the production of light nuclei in the framework of the nucleon coalescence. We present in particular the analytic expressions for the coalescence factors  $B_2$  and  $B_3$  measured by RHIC and LHC experiments [40–42,45–51] and discuss their qualitative properties. In Sec. III, we apply the deduced results to  $p$ - $p$ ,  $p$ -Pb, and Pb-Pb collisions at the LHC. In Sec. IV, we give a summary.

## II. FORMULAS OF LIGHT NUCLEI PRODUCTION IN THE COALESCENCE MECHANISM

In this section we start from the basic ideas of coalescence and present general formulas of momentum dependence of light nuclei. Then we present the results obtained with several assumptions and/or approximations, such as the factorization of coordinate and momentum, and those in modeling normalized nucleon coordinate distribution. Finally, we give analytic results of coalescence factors  $B_2$  and  $B_3$  as functions of the system size and the momentum of light nuclei and discuss their features.

### A. The general formalism

We start with a hadronic system produced at the final stage of the evolution of high-energy collision and suppose light nuclei are formed via nucleon coalescence. The three-dimensional momentum distribution of the produced deuterons  $f_d(\mathbf{p})$  and that of helions  $f_{^3\text{He}}(\mathbf{p})$  are given by

$$f_d(\mathbf{p}) = \int d\mathbf{x}_1 d\mathbf{x}_2 d\mathbf{p}_1 d\mathbf{p}_2 f_{pn}(\mathbf{x}_1, \mathbf{x}_2; \mathbf{p}_1, \mathbf{p}_2) \times \mathcal{R}_d(\mathbf{x}_1, \mathbf{x}_2; \mathbf{p}_1, \mathbf{p}_2, \mathbf{p}), \quad (2)$$

$$f_{^3\text{He}}(\mathbf{p}) = \int d\mathbf{x}_1 d\mathbf{x}_2 d\mathbf{x}_3 d\mathbf{p}_1 d\mathbf{p}_2 d\mathbf{p}_3 f_{ppn}(\mathbf{x}_1, \mathbf{x}_2, \mathbf{x}_3; \mathbf{p}_1, \mathbf{p}_2, \mathbf{p}_3) \times \mathcal{R}_{^3\text{He}}(\mathbf{x}_1, \mathbf{x}_2, \mathbf{x}_3; \mathbf{p}_1, \mathbf{p}_2, \mathbf{p}_3, \mathbf{p}), \quad (3)$$

where  $f_{pn}(\mathbf{x}_1, \mathbf{x}_2; \mathbf{p}_1, \mathbf{p}_2)$  and  $f_{ppn}(\mathbf{x}_1, \mathbf{x}_2, \mathbf{x}_3; \mathbf{p}_1, \mathbf{p}_2, \mathbf{p}_3)$  are two- and three-nucleon joint coordinate-momentum distributions, respectively, and  $\mathcal{R}_d(\mathbf{x}_1, \mathbf{x}_2; \mathbf{p}_1, \mathbf{p}_2, \mathbf{p})$  and  $\mathcal{R}_{^3\text{He}}(\mathbf{x}_1, \mathbf{x}_2, \mathbf{x}_3; \mathbf{p}_1, \mathbf{p}_2, \mathbf{p}_3, \mathbf{p})$  are kernel functions. Here and from now on we use bold symbols to denote three-dimensional coordinates and momenta.

The joint coordinate-momentum distributions  $f_{pn}(\mathbf{x}_1, \mathbf{x}_2; \mathbf{p}_1, \mathbf{p}_2)$  and  $f_{ppn}(\mathbf{x}_1, \mathbf{x}_2, \mathbf{x}_3; \mathbf{p}_1, \mathbf{p}_2, \mathbf{p}_3)$  are the nucleon number densities. They satisfy

$$\int f_{pn}(\mathbf{x}_1, \mathbf{x}_2; \mathbf{p}_1, \mathbf{p}_2) d\mathbf{x}_1 d\mathbf{x}_2 d\mathbf{p}_1 d\mathbf{p}_2 = N_{pn}, \quad (4)$$

$$\int f_{ppn}(\mathbf{x}_1, \mathbf{x}_2, \mathbf{x}_3; \mathbf{p}_1, \mathbf{p}_2, \mathbf{p}_3) d\mathbf{x}_1 d\mathbf{x}_2 d\mathbf{x}_3 d\mathbf{p}_1 d\mathbf{p}_2 d\mathbf{p}_3 = N_{ppn}, \quad (5)$$

where  $N_{pn} = N_p N_n$  and  $N_{ppn} = N_p(N_p - 1)N_n$  are the number of all possible  $pn$  pairs and that of all possible  $ppn$  clusters, respectively.  $N_p$  is the number of protons and  $N_n$  is that of neutrons in the considered hadronic system. We can rewrite the

joint distributions in terms of the normalized forms denoted by the superscript ( $n$ ) as

$$f_{pn}(\mathbf{x}_1, \mathbf{x}_2; \mathbf{p}_1, \mathbf{p}_2) = N_{pn} f_{pn}^{(n)}(\mathbf{x}_1, \mathbf{x}_2; \mathbf{p}_1, \mathbf{p}_2), \quad (6)$$

$$f_{ppn}(\mathbf{x}_1, \mathbf{x}_2, \mathbf{x}_3; \mathbf{p}_1, \mathbf{p}_2, \mathbf{p}_3) = N_{ppn} f_{ppn}^{(n)}(\mathbf{x}_1, \mathbf{x}_2, \mathbf{x}_3; \mathbf{p}_1, \mathbf{p}_2, \mathbf{p}_3). \quad (7)$$

Kernel functions  $\mathcal{R}_d(\mathbf{x}_1, \mathbf{x}_2; \mathbf{p}_1, \mathbf{p}_2, \mathbf{p})$  and  $\mathcal{R}_{^3\text{He}}(\mathbf{x}_1, \mathbf{x}_2, \mathbf{x}_3; \mathbf{p}_1, \mathbf{p}_2, \mathbf{p}_3, \mathbf{p})$  denote the probability density for  $p, n$  with momenta  $\mathbf{p}_1$  and  $\mathbf{p}_2$  at  $\mathbf{x}_1$  and  $\mathbf{x}_2$  to recombine into a  $d$  of momentum  $\mathbf{p}$ , and that for  $p, p, n$  with momenta  $\mathbf{p}_1, \mathbf{p}_2$ , and  $\mathbf{p}_3$  at  $\mathbf{x}_1, \mathbf{x}_2$ , and  $\mathbf{x}_3$  to recombine into a  $^3\text{He}$  of momentum  $\mathbf{p}$ , respectively. Just as discussed in Ref. [55], they carry the kinetic and dynamical information of the nucleons recombining into light nuclei, and their precise expressions should be constrained by such as the momentum conservation, constraints due to intrinsic quantum numbers, e.g., spin, and so on. To take these constraints into account explicitly, we rewrite them in the following forms:

$$\mathcal{R}_d(\mathbf{x}_1, \mathbf{x}_2; \mathbf{p}_1, \mathbf{p}_2, \mathbf{p}) = g_d \mathcal{R}_d^{(x,p)}(\mathbf{x}_1, \mathbf{x}_2; \mathbf{p}_1, \mathbf{p}_2) \delta\left(\sum_{i=1}^2 \mathbf{p}_i - \mathbf{p}\right), \quad (8)$$

$$\mathcal{R}_{^3\text{He}}(\mathbf{x}_1, \mathbf{x}_2, \mathbf{x}_3; \mathbf{p}_1, \mathbf{p}_2, \mathbf{p}_3, \mathbf{p}) = g_{^3\text{He}} \mathcal{R}_{^3\text{He}}^{(x,p)}(\mathbf{x}_1, \mathbf{x}_2, \mathbf{x}_3; \mathbf{p}_1, \mathbf{p}_2, \mathbf{p}_3) \delta\left(\sum_{i=1}^3 \mathbf{p}_i - \mathbf{p}\right), \quad (9)$$

where the spin degeneracy factors  $g_d = 3/4$  and  $g_{^3\text{He}} = 1/4$ . The Dirac  $\delta$  functions guarantee momentum conservation in the coalescence. The remaining  $\mathcal{R}_d^{(x,p)}(\mathbf{x}_1, \mathbf{x}_2; \mathbf{p}_1, \mathbf{p}_2)$  now stands for the probability of a  $pn$  pair with momenta  $\mathbf{p}_1$  and  $\mathbf{p}_2$  at  $\mathbf{x}_1$  and  $\mathbf{x}_2$  to recombine into a composite  $d$ -like particle with any momentum and any spin quantum number and similarly for  $\mathcal{R}_{^3\text{He}}^{(x,p)}(\mathbf{x}_1, \mathbf{x}_2, \mathbf{x}_3; \mathbf{p}_1, \mathbf{p}_2, \mathbf{p}_3)$ . They depend on the positions and momenta of the nucleons and should be determined by the dynamics in the coalescence process.

In this way, we obtain the momentum distribution of  $d$  and that of  $^3\text{He}$  as

$$f_d(\mathbf{p}) = g_d N_{pn} \int d\mathbf{x}_1 d\mathbf{x}_2 d\mathbf{p}_1 d\mathbf{p}_2 f_{pn}^{(n)}(\mathbf{x}_1, \mathbf{x}_2; \mathbf{p}_1, \mathbf{p}_2) \times \mathcal{R}_d^{(x,p)}(\mathbf{x}_1, \mathbf{x}_2; \mathbf{p}_1, \mathbf{p}_2) \delta\left(\sum_{i=1}^2 \mathbf{p}_i - \mathbf{p}\right), \quad (10)$$

$$f_{^3\text{He}}(\mathbf{p}) = g_{^3\text{He}} N_{ppn} \int d\mathbf{x}_1 d\mathbf{x}_2 d\mathbf{x}_3 d\mathbf{p}_1 d\mathbf{p}_2 d\mathbf{p}_3 \times f_{ppn}^{(n)}(\mathbf{x}_1, \mathbf{x}_2, \mathbf{x}_3; \mathbf{p}_1, \mathbf{p}_2, \mathbf{p}_3) \times \mathcal{R}_{^3\text{He}}^{(x,p)}(\mathbf{x}_1, \mathbf{x}_2, \mathbf{x}_3; \mathbf{p}_1, \mathbf{p}_2, \mathbf{p}_3) \delta\left(\sum_{i=1}^3 \mathbf{p}_i - \mathbf{p}\right). \quad (11)$$

Equations (10) and (11) are the general formulas for studying momentum distributions of light nuclei based on the basic ideas of the coalescence mechanism. More specific results can be obtained when special assumptions or approximations are

made about the normalized nucleon joint distributions and/or the coordinate-momentum-dependent kernel functions.

### B. Factorization of coordinate and momentum dependencies

Generally, the coordinate and momentum dependencies of kernel functions and nucleon joint distributions are coupled to each other, especially in relativistic heavy-ion collisions where the collective expansion exists. The coupling intensities and its specific forms are probably different in different collision systems and centralities. Such coupling effects on light nuclei production have been studied in Refs. [21,22]. In this article, we focus on common features for production mechanisms of light nuclei in  $p$ - $p$ ,  $p$ - $A$ , and  $A$ - $A$  collisions, and in particular for a consistent understanding for the collision system size and momentum dependencies of the coalescence factor  $B_A$ . We try our best to derive production formulas analytically and present momentum and collision system de-

pendencies of light nuclei more intuitively, so we do not include such coordinate-momentum coupling. We consider only this case where the coordinate and momentum dependencies of kernel functions are decoupled from each other, i.e.,

$$\mathcal{R}_d^{(x,p)}(\mathbf{x}_1, \mathbf{x}_2; \mathbf{p}_1, \mathbf{p}_2) = \mathcal{R}_d^{(x)}(\mathbf{x}_1, \mathbf{x}_2)\mathcal{R}_d^{(p)}(\mathbf{p}_1, \mathbf{p}_2), \quad (12)$$

$$\begin{aligned} \mathcal{R}_{3\text{He}}^{(x,p)}(\mathbf{x}_1, \mathbf{x}_2, \mathbf{x}_3; \mathbf{p}_1, \mathbf{p}_2, \mathbf{p}_3) &= \mathcal{R}_{3\text{He}}^{(x)}(\mathbf{x}_1, \mathbf{x}_2, \mathbf{x}_3) \\ &\times \mathcal{R}_{3\text{He}}^{(p)}(\mathbf{p}_1, \mathbf{p}_2, \mathbf{p}_3), \end{aligned} \quad (13)$$

and the normalized joint distributions of the nucleons are coordinate and momentum factorized as follows:

$$f_{pn}^{(n)}(\mathbf{x}_1, \mathbf{x}_2; \mathbf{p}_1, \mathbf{p}_2) = f_{pn}^{(n)}(\mathbf{x}_1, \mathbf{x}_2)f_{pn}^{(n)}(\mathbf{p}_1, \mathbf{p}_2), \quad (14)$$

$$f_{ppn}^{(n)}(\mathbf{x}_1, \mathbf{x}_2, \mathbf{x}_3; \mathbf{p}_1, \mathbf{p}_2, \mathbf{p}_3) = f_{ppn}^{(n)}(\mathbf{x}_1, \mathbf{x}_2, \mathbf{x}_3)f_{ppn}^{(n)}(\mathbf{p}_1, \mathbf{p}_2, \mathbf{p}_3). \quad (15)$$

Substituting Eqs. (12)–(15) into Eqs. (10) and (11), we have

$$f_d(\mathbf{p}) = g_d N_{pn} \int d\mathbf{x}_1 d\mathbf{x}_2 f_{pn}^{(n)}(\mathbf{x}_1, \mathbf{x}_2) \mathcal{R}_d^{(x)}(\mathbf{x}_1, \mathbf{x}_2) \int d\mathbf{p}_1 d\mathbf{p}_2 f_{pn}^{(n)}(\mathbf{p}_1, \mathbf{p}_2) \mathcal{R}_d^{(p)}(\mathbf{p}_1, \mathbf{p}_2) \delta\left(\sum_{i=1}^2 \mathbf{p}_i - \mathbf{p}\right), \quad (16)$$

$$f_{3\text{He}}(\mathbf{p}) = g_{3\text{He}} N_{ppn} \int d\mathbf{x}_1 d\mathbf{x}_2 d\mathbf{x}_3 f_{ppn}^{(n)}(\mathbf{x}_1, \mathbf{x}_2, \mathbf{x}_3) \mathcal{R}_{3\text{He}}^{(x)}(\mathbf{x}_1, \mathbf{x}_2, \mathbf{x}_3) \int d\mathbf{p}_1 d\mathbf{p}_2 d\mathbf{p}_3 f_{ppn}^{(n)}(\mathbf{p}_1, \mathbf{p}_2, \mathbf{p}_3) \mathcal{R}_{3\text{He}}^{(p)}(\mathbf{p}_1, \mathbf{p}_2, \mathbf{p}_3) \delta\left(\sum_{i=1}^3 \mathbf{p}_i - \mathbf{p}\right). \quad (17)$$

Equations (16) and (17) show that we can calculate momentum distributions of different light nuclei by integrating coordinates and momenta of nucleons, respectively.

We use  $\mathcal{A}_d$  and  $\mathcal{A}_{3\text{He}}$  to denote the coordinate integral parts in Eqs. (16) and (17) as

$$\mathcal{A}_d = \int d\mathbf{x}_1 d\mathbf{x}_2 f_{pn}^{(n)}(\mathbf{x}_1, \mathbf{x}_2) \mathcal{R}_d^{(x)}(\mathbf{x}_1, \mathbf{x}_2), \quad (18)$$

$$\mathcal{A}_{3\text{He}} = \int d\mathbf{x}_1 d\mathbf{x}_2 d\mathbf{x}_3 f_{ppn}^{(n)}(\mathbf{x}_1, \mathbf{x}_2, \mathbf{x}_3) \mathcal{R}_{3\text{He}}^{(x)}(\mathbf{x}_1, \mathbf{x}_2, \mathbf{x}_3), \quad (19)$$

and use  $\mathcal{M}_d(\mathbf{p})$  and  $\mathcal{M}_{3\text{He}}(\mathbf{p})$  to denote the momentum integral parts as

$$\mathcal{M}_d(\mathbf{p}) = \int d\mathbf{p}_1 d\mathbf{p}_2 f_{pn}^{(n)}(\mathbf{p}_1, \mathbf{p}_2) \mathcal{R}_d^{(p)}(\mathbf{p}_1, \mathbf{p}_2) \delta\left(\sum_{i=1}^2 \mathbf{p}_i - \mathbf{p}\right), \quad (20)$$

$$\begin{aligned} \mathcal{M}_{3\text{He}}(\mathbf{p}) &= \int d\mathbf{p}_1 d\mathbf{p}_2 d\mathbf{p}_3 f_{ppn}^{(n)}(\mathbf{p}_1, \mathbf{p}_2, \mathbf{p}_3) \mathcal{R}_{3\text{He}}^{(p)}(\mathbf{p}_1, \mathbf{p}_2, \mathbf{p}_3) \\ &\times \delta\left(\sum_{i=1}^3 \mathbf{p}_i - \mathbf{p}\right). \end{aligned} \quad (21)$$

So we get

$$f_d(\mathbf{p}) = g_d N_{pn} \mathcal{A}_d \mathcal{M}_d(\mathbf{p}), \quad (22)$$

$$f_{3\text{He}}(\mathbf{p}) = g_{3\text{He}} N_{ppn} \mathcal{A}_{3\text{He}} \mathcal{M}_{3\text{He}}(\mathbf{p}). \quad (23)$$

$\mathcal{A}_d$  stands for the probability of a  $pn$  pair satisfying the coordinate requirement to recombine into a deuteron-like

molecular state, and  $\mathcal{M}_d(\mathbf{p})$  stands for the probability of a  $pn$  pair satisfying the momentum requirement to recombine into a deuteron-like molecular state with momentum  $\mathbf{p}$ . The similar case holds for  $\mathcal{A}_{3\text{He}}$  and  $\mathcal{M}_{3\text{He}}(\mathbf{p})$ . To evaluate these  $\mathcal{A}_{d/3\text{He}}$  and  $\mathcal{M}_{d/3\text{He}}(\mathbf{p})$ , we need the coordinate and momentum factorized kernel functions and nucleon distributions. In the following, we model their precise forms and give the corresponding analytic formulas for momentum distributions of light nuclei.

### C. Forms of kernel functions

With the instantaneous coalescence approximation, kernel functions can be solved from the Wigner transformation once the wave functions of the light nuclei are given. Just as in coalescence models in Refs. [56,57], we adopt the wave function of a spherical harmonic oscillator and get the coordinate and momentum factorized Gaussian forms for our kernel functions. Note that kernel functions should be directly determined by the relative coordinates and relative momenta of the primordial nucleons in the  $pn$ -pair (or  $ppn$ -cluster) rest frame rather than those in the laboratory frame [3]. So we have

$$\mathcal{R}_d^{(x)}(\mathbf{x}_1, \mathbf{x}_2) = 8e^{-\frac{(x'_1 - x'_2)^2}{\sigma_d^2}}, \quad (24)$$

$$\mathcal{R}_d^{(p)}(\mathbf{p}_1, \mathbf{p}_2) = e^{-\frac{\sigma_d^2(p'_1 - p'_2)^2}{4\hbar^2 c^2}}, \quad (25)$$

$$\mathcal{R}_{3\text{He}}^{(x)}(\mathbf{x}_1, \mathbf{x}_2, \mathbf{x}_3) = 8^2 e^{-\frac{(x'_1 - x'_2)^2}{2\sigma_{3\text{He}}^2}} e^{-\frac{(x'_1 + x'_2 - 2x'_3)^2}{6\sigma_{3\text{He}}^2}}, \quad (26)$$

$$\mathcal{R}_{3\text{He}}^{(p)}(\mathbf{p}_1, \mathbf{p}_2, \mathbf{p}_3) = e^{-\frac{\sigma_{3\text{He}}^2(p'_1 - p'_2)^2}{2\hbar^2 c^2}} e^{-\frac{\sigma_{3\text{He}}^2(p'_1 + p'_2 - 2p'_3)^2}{6\hbar^2 c^2}}. \quad (27)$$

Here, as well as in the rest of this article, the superscript “ $\prime$ ” in the coordinate or momentum variable denotes the coordinate or momentum of the nucleon in the rest frame of the  $pn$ -pair or  $ppn$ -cluster. The width parameter  $\sigma_d = \sqrt{\frac{8}{3}}R_d$  and  $\sigma_{^3\text{He}} = R_{^3\text{He}}$ , where  $R_d$  and  $R_{^3\text{He}}$  are the root-mean-square radius of the deuteron and that of the  $^3\text{He}$ , respectively. The factor  $\hbar c$  comes from the GeV fm unit used, and it is 0.197 GeV fm.

#### D. Modeling the normalized coordinate distribution

In this section we calculate  $\mathcal{A}_d$  and  $\mathcal{A}_{^3\text{He}}$ . Changing coordinate integral variables in Eq. (18) to be  $\mathbf{X}_C = \frac{\mathbf{x}_1 + \mathbf{x}_2}{2}$  and  $\mathbf{r} = \mathbf{x}_1 - \mathbf{x}_2$ , and those in Eq. (19) to be  $\mathbf{Y}_C = (\mathbf{x}_1 + \mathbf{x}_2 + \mathbf{x}_3)/\sqrt{3}$ ,  $\mathbf{r}_1 = (\mathbf{x}_1 - \mathbf{x}_2)/\sqrt{2}$ , and  $\mathbf{r}_2 = (\mathbf{x}_1 + \mathbf{x}_2 - 2\mathbf{x}_3)/\sqrt{6}$ , and recalling Eqs. (24) and (26), we have

$$\mathcal{A}_d = 8 \int d\mathbf{X}_C d\mathbf{r} f_{pn}^{(n)}(\mathbf{X}_C, \mathbf{r}) e^{-\frac{r^2}{\sigma_d^2}}, \quad (28)$$

$$\mathcal{A}_{^3\text{He}} = 8^2 \int d\mathbf{Y}_C d\mathbf{r}_1 d\mathbf{r}_2 f_{ppn}^{(n)}(\mathbf{Y}_C, \mathbf{r}_1, \mathbf{r}_2) e^{-\frac{(r_1^2 + r_2^2)}{\sigma_{^3\text{He}}^2}}. \quad (29)$$

The normalization conditions become

$$\int f_{pn}^{(n)}(\mathbf{X}_C, \mathbf{r}) d\mathbf{X}_C d\mathbf{r} = 1. \quad (30)$$

$$\int f_{ppn}^{(n)}(\mathbf{Y}_C, \mathbf{r}_1, \mathbf{r}_2) d\mathbf{Y}_C d\mathbf{r}_1 d\mathbf{r}_2 = 1. \quad (31)$$

We further assume the coordinate joint distributions are coordinate variable factorized, i.e.,  $f_{pn}^{(n)}(\mathbf{X}_C, \mathbf{r}) = f_{pn}^{(n)}(\mathbf{X}_C) f_{pn}^{(n)}(\mathbf{r})$  and  $f_{ppn}^{(n)}(\mathbf{Y}_C, \mathbf{r}_1, \mathbf{r}_2) = f_{ppn}^{(n)}(\mathbf{Y}_C) f_{ppn}^{(n)}(\mathbf{r}_1) f_{ppn}^{(n)}(\mathbf{r}_2)$ . Then we have

$$\mathcal{A}_d = 8 \int d\mathbf{r} f_{pn}^{(n)}(\mathbf{r}) e^{-\frac{r^2}{\sigma_d^2}}, \quad (32)$$

$$\mathcal{A}_{^3\text{He}} = 8^2 \int d\mathbf{r}_1 d\mathbf{r}_2 f_{ppn}^{(n)}(\mathbf{r}_1) f_{ppn}^{(n)}(\mathbf{r}_2) e^{-\frac{(r_1^2 + r_2^2)}{\sigma_{^3\text{He}}^2}}. \quad (33)$$

As in Ref. [58], we adopt

$$f_{pn}^{(n)}(\mathbf{r}) = \frac{1}{(\pi C R_f^2)^{1.5}} e^{-\frac{r^2}{C R_f^2}},$$

$$f_{ppn}^{(n)}(\mathbf{r}_1) = \frac{1}{(\pi C_1 R_f^2)^{1.5}} e^{-\frac{r_1^2}{C_1 R_f^2}},$$

$$f_{ppn}^{(n)}(\mathbf{r}_2) = \frac{1}{(\pi C_2 R_f^2)^{1.5}} e^{-\frac{r_2^2}{C_2 R_f^2}},$$

where  $R_f$  is the effective radius of the source system at the light nuclei freeze-out and  $C$ ,  $C_1$ , and  $C_2$  are distribution width parameters. Considering relations between  $\mathbf{r}$ ,  $\mathbf{r}_1$ , and  $\mathbf{r}_2$  with  $\mathbf{x}_1$ ,  $\mathbf{x}_2$ , and  $\mathbf{x}_3$ ,  $C_1$  should be equal to  $C/2$  and  $C_2$  should be equal to  $2C/3$ . So there is only one distribution width parameter  $C$  to be determined. In this article we set it to be four, the same as in Ref. [58].

The Lorentz transformation gives  $\mathbf{x} = \mathbf{x}' + (\gamma - 1)\frac{\mathbf{x}' \cdot \boldsymbol{\beta}}{\beta^2} \boldsymbol{\beta} + \gamma t' \boldsymbol{\beta}$ , where  $\gamma = 1/(1 - \beta^2)^{1/2}$  and  $\boldsymbol{\beta}$  is the velocity of the

center of mass of the  $pn$  pair or  $ppn$  cluster in the laboratory frame. Considering instantaneous coalescence in the rest frame of the  $pn$  pair or  $ppn$  cluster, i.e.,  $\Delta t' = 0$ , we get

$$\mathbf{r} = \mathbf{r}' + (\gamma - 1)\frac{\mathbf{r}' \cdot \boldsymbol{\beta}}{\beta^2} \boldsymbol{\beta}. \quad (34)$$

Substituting the above equation into Eqs. (32) and (33) and integrating from relative coordinate variables, we obtain

$$\mathcal{A}_d = \frac{8\sigma_d^3}{(C R_f^2 + \sigma_d^2)\sqrt{C(R_f/\gamma)^2 + \sigma_d^2}}, \quad (35)$$

$$\begin{aligned} \mathcal{A}_{^3\text{He}} &= \frac{8\sigma_{^3\text{He}}^3}{(\frac{C}{2}R_f^2 + \sigma_{^3\text{He}}^2)\sqrt{\frac{C}{2}(R_f/\gamma)^2 + \sigma_{^3\text{He}}^2}} \\ &\times \frac{8\sigma_{^3\text{He}}^3}{(\frac{2C}{3}R_f^2 + \sigma_{^3\text{He}}^2)\sqrt{\frac{2C}{3}(R_f/\gamma)^2 + \sigma_{^3\text{He}}^2}}. \end{aligned} \quad (36)$$

The above two equations show that the coalescence probability in coordinate space becomes larger when applying coalescence criteria in the rest frame of the forming light nuclei compared with applying them in the laboratory frame where  $\gamma = 1$ . This can be equivalently understood as that the size of the fireball formed in the laboratory is Lorentz contracted in the rest frame of the forming light nuclei, so the mean relative distance between nucleons becomes smaller and the coalescence becomes easier.

#### E. Evaluating the nucleon momentum integral

In this section, we evaluate  $\mathcal{M}_d(\mathbf{p})$  and  $\mathcal{M}_{^3\text{He}}(\mathbf{p})$ . Substituting Eqs. (25) and (27) into Eqs. (20) and (21), we have

$$\mathcal{M}_d(\mathbf{p}) = \int d\mathbf{p}_1 d\mathbf{p}_2 f_{pn}^{(n)}(\mathbf{p}_1, \mathbf{p}_2) e^{-\frac{\sigma_d^2(\mathbf{p}'_1 - \mathbf{p}'_2)^2}{4\hbar^2 c^2}} \delta\left(\sum_{i=1}^2 \mathbf{p}_i - \mathbf{p}\right), \quad (37)$$

$$\begin{aligned} \mathcal{M}_{^3\text{He}}(\mathbf{p}) &= \int d\mathbf{p}_1 d\mathbf{p}_2 d\mathbf{p}_3 f_{ppn}^{(n)}(\mathbf{p}_1, \mathbf{p}_2, \mathbf{p}_3) e^{-\frac{\sigma_{^3\text{He}}^2(\mathbf{p}'_1 - \mathbf{p}'_2)^2}{2\hbar^2 c^2}} \\ &\times e^{-\frac{\sigma_{^3\text{He}}^2(\mathbf{p}'_1 + \mathbf{p}'_2 - 2\mathbf{p}'_3)^2}{6\hbar^2 c^2}} \delta\left(\sum_{i=1}^3 \mathbf{p}_i - \mathbf{p}\right). \end{aligned} \quad (38)$$

Exact evaluations of  $\mathcal{M}_d$  and  $\mathcal{M}_{^3\text{He}}$  need the precise forms of nucleon joint momentum distributions, which depend on collision environments such as collision system, collision energy, collision centrality, etc. In this situation, the accurately analytic results for integrals in Eqs. (37) and (38) are usually difficult to obtain. To get intuitionistic expressions for momentum dependence of light nuclei, in particular, those for  $B_A$  factors, here we adopt the following mathematical

approximation. Recalling that  $\sigma_d = \sqrt{\frac{8}{3}}R_d$  and  $\sigma_{^3\text{He}} = R_{^3\text{He}}$ , where the root-mean-square charge radius of the deuteron  $R_d = 2.1421$  fm and that of the  $^3\text{He}$   $R_{^3\text{He}} = 1.9661$  fm [59], we see that the Gaussian width values  $2\hbar c/\sigma_d$ ,  $\sqrt{2}\hbar c/\sigma_{^3\text{He}}$ , and  $\sqrt{6}\hbar c/\sigma_{^3\text{He}}$  in Eqs. (37) and (38) are quite small. So we can mathematically approximate the Gaussian form of the kernel function  $e^{-(\Delta\mathbf{p}')^2/\epsilon^2}$  as  $(\sqrt{\pi}\epsilon)^3\delta(\Delta\mathbf{p}')$ , where  $\epsilon$  is a small quantity. Then we immediately obtain

$$\begin{aligned}\mathcal{M}_d(\mathbf{p}) &= \left(\frac{2\hbar c}{\sigma_d}\sqrt{\pi}\right)^3 \int d\mathbf{p}_1 d\mathbf{p}_2 f_{pm}^{(n)}(\mathbf{p}_1, \mathbf{p}_2) \delta(\mathbf{p}'_1 - \mathbf{p}'_2) \\ &\quad \times \delta\left(\sum_{i=1}^2 \mathbf{p}_i - \mathbf{p}_d\right) \\ &= \left(\frac{2\hbar c}{\sigma_d}\sqrt{\pi}\right)^3 \int d\mathbf{p}_1 d\mathbf{p}_2 f_{pm}^{(n)}(\mathbf{p}_1, \mathbf{p}_2) \gamma \delta(\mathbf{p}_1 - \mathbf{p}_2) \\ &\quad \times \delta\left(\sum_{i=1}^2 \mathbf{p}_i - \mathbf{p}_d\right) \\ &= \left(\frac{\hbar c}{\sigma_d}\sqrt{\pi}\right)^3 \gamma f_{pm}^{(n)}\left(\frac{\mathbf{p}}{2}, \frac{\mathbf{p}}{2}\right),\end{aligned}\quad (39)$$

where  $\gamma$  comes from  $\Delta\mathbf{p}' = \frac{1}{\gamma}\Delta\mathbf{p}$ . Similarly we get

$$\mathcal{M}_{^3\text{He}}(\mathbf{p}) = \left(\frac{\pi\hbar^2 c^2}{\sqrt{3}\sigma_{^3\text{He}}^2}\right)^3 \gamma^2 f_{ppn}^{(n)}\left(\frac{\mathbf{p}}{3}, \frac{\mathbf{p}}{3}, \frac{\mathbf{p}}{3}\right). \quad (40)$$

Ignoring correlations between protons and neutrons, we finally have

$$\mathcal{M}_d(\mathbf{p}) = \left(\frac{\hbar c}{\sigma_d}\sqrt{\pi}\right)^3 \gamma f_p^{(n)}\left(\frac{\mathbf{p}}{2}\right) f_n^{(n)}\left(\frac{\mathbf{p}}{2}\right), \quad (41)$$

$$\mathcal{M}_{^3\text{He}}(\mathbf{p}) = \left(\frac{\pi\hbar^2 c^2}{\sqrt{3}\sigma_{^3\text{He}}^2}\right)^3 \gamma^2 f_p^{(n)}\left(\frac{\mathbf{p}}{3}\right) f_p^{(n)}\left(\frac{\mathbf{p}}{3}\right) f_n^{(n)}\left(\frac{\mathbf{p}}{3}\right). \quad (42)$$

To check the robustness of the above  $\delta$ -function approximation, we also take a classical Boltzmann distribution  $f_{p,n}^{(n)} = \frac{1}{(2\pi mT)^{1.5}} e^{-p^2/(2mT)}$  for nucleons as an example to carry out practical integrals in Eqs. (37) and (38). We can obtain the exact results of momentum integrals. Considering the relationship  $mT\sigma_{d/^3\text{He}}^2 \gg \gamma^2\hbar^2 c^2$ , we can express integrated results as Taylor series and the leading terms are just Eqs. (41) and (42).

### F. Momentum distributions of light nuclei

Substituting Eqs. (35), (36) and (41), (42) into Eqs. (22) and (23), we finally have the momentum distributions of light nuclei as

$$f_d(\mathbf{p}) = \frac{8(\sqrt{\pi}\hbar c)^3 g_d \gamma}{(CR_f^2 + \sigma_d^2)\sqrt{C(R_f/\gamma)^2 + \sigma_d^2}} f_p\left(\frac{\mathbf{p}}{2}\right) f_n\left(\frac{\mathbf{p}}{2}\right), \quad (43)$$

$$\begin{aligned}f_{^3\text{He}}(\mathbf{p}) &= \frac{8^2(\pi\hbar^2 c^2)^3 g_{^3\text{He}} \gamma^2}{3\sqrt{3}\left(\frac{C}{2}R_f^2 + \sigma_{^3\text{He}}^2\right)\sqrt{\frac{C}{2}(R_f/\gamma)^2 + \sigma_{^3\text{He}}^2}} \\ &\quad \times \frac{1}{\left(\frac{2C}{3}R_f^2 + \sigma_{^3\text{He}}^2\right)\sqrt{\frac{2C}{3}(R_f/\gamma)^2 + \sigma_{^3\text{He}}^2}} \\ &\quad \times f_p\left(\frac{\mathbf{p}}{3}\right) f_p\left(\frac{\mathbf{p}}{3}\right) f_n\left(\frac{\mathbf{p}}{3}\right).\end{aligned}\quad (44)$$

Equations (43) and (44) show the relationships of light nuclei with primordial nucleons in momentum space in the laboratory frame. They can be used to calculate the yields and transverse momentum spectra of light nuclei measured extensively as long as the nucleon momentum distributions are given. They can also be conveniently used to probe production correlations of light nuclei and nucleons, such as the coalescence factor, which will be discussed in the next section.

### G. Coalescence factor $B_A$

In this section, we explore analytic results of coalescence factors  $B_A$ . Noting that in Eq. (43)  $f_d(\mathbf{p}) = d^3 N_d/d\mathbf{p}_d$  and  $f_{p,n}(\mathbf{p}) = d^3 N_{p,n}/d\mathbf{p}_{p,n}$ , we have

$$\begin{aligned}B_2 &\equiv \left(E_d \frac{d^3 N_d}{d\mathbf{p}_d}\right) / \left[\left(E_p \frac{d^3 N_p}{d\mathbf{p}_p}\right) \left(E_n \frac{d^3 N_n}{d\mathbf{p}_n}\right)\right] \\ &= \frac{32(\sqrt{\pi}\hbar c)^3 g_d}{m_d(CR_f^2 + \sigma_d^2)\sqrt{C(R_f/\gamma)^2 + \sigma_d^2}},\end{aligned}\quad (45)$$

where  $E_p = E_n = \frac{1}{2}E_d = \frac{1}{2}\gamma m_d$  is used for the second equality. The mass of the deuteron is  $m_d = 1.875$  GeV and  $\gamma = (1 + \mathbf{p}_d^2/m_d^2)^{1/2}$ . Our result Eq. (45) is consistent with previous works [22,25], as one notices that we define  $R_f$  in the laboratory frame while Refs. [25] and [22] defined these fireball radius parameters in the nucleon pair rest frame and the Yano-Koonin-Podgoretski (YKP) frame, respectively.

Similarly for  $^3\text{He}$ , we have

$$\begin{aligned}B_3 &= \frac{192\sqrt{3}(\pi\hbar^2 c^2)^3 g_{^3\text{He}}}{m_{^3\text{He}}^2 \left(\frac{C}{2}R_f^2 + \sigma_{^3\text{He}}^2\right)\sqrt{\frac{C}{2}(R_f/\gamma)^2 + \sigma_{^3\text{He}}^2}} \\ &\quad \times \frac{1}{\left(\frac{2C}{3}R_f^2 + \sigma_{^3\text{He}}^2\right)\sqrt{\frac{2C}{3}(R_f/\gamma)^2 + \sigma_{^3\text{He}}^2}}.\end{aligned}\quad (46)$$

The mass of  $^3\text{He}$  is  $m_{^3\text{He}} = 2.815$  GeV and  $\gamma = (1 + \mathbf{p}_{^3\text{He}}^2/m_{^3\text{He}}^2)^{1/2}$ . Equations (45) and (46) are the final results for  $B_A$  factors we derived, which clearly show that  $B_2$  and  $B_3$  depend sensitively on the system size denoted by  $R_f$ , the size of light nuclei via  $\sigma_{d/^3\text{He}}$ , and the momentum of light nuclei via  $\gamma$ .

From Eqs. (45) and (46), we can get properties of  $B_A$  factors. The first is the larger  $R_f$ , the smaller  $B_2$ , and  $B_3$ . This means  $B_A$  always becomes smaller from small  $p$ - $p$  collisions to semicentral Pb-Pb collisions and then to central Pb-Pb collisions. The second is that finite sizes of light nuclei suppress their production, and the suppression is stronger in small  $p$ - $p$  and  $p$ -Pb collisions than in Pb-Pb collisions. Last but not most important, Eqs. (45) and (46) give explicitly the momentum

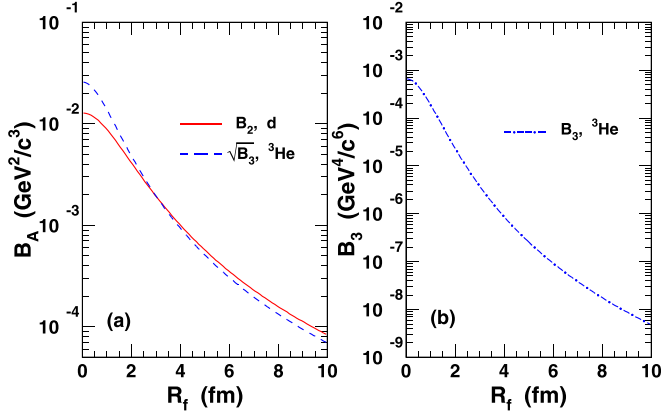


FIG. 1. (a)  $B_2$  of  $d$  and  $\sqrt{B_3}$  of  ${}^3\text{He}$ , (b)  $B_3$  of  ${}^3\text{He}$  as a function of  $R_f$  at  $p_T/A = 0.75$  GeV/ $c$ .

dependence of  $B_2$  and  $B_3$  via  $\gamma$ . In the case of  $R_f \gg \sigma_d$  or  $\sigma_{{}^3\text{He}}$ , such as in central Pb-Pb collisions at the LHC, both  $B_2$  and  $B_3$  increase with the increasing momentum. In the case of  $R_f \ll \sigma_d$  or  $\sigma_{{}^3\text{He}}$ , such as in small  $p$ - $p$  collisions,  $B_2$  and  $B_3$  nearly keep invariant with the momentum. All these properties of  $B_A$  are characteristics of light nuclei production in the coalescence production mechanism. They can be directly tested by the experimental data.

### III. APPLICATIONS IN $p$ - $p$ , $p$ -Pb, AND Pb-Pb COLLISIONS AT THE LARGE HADRON COLLIDER

In this section, we apply the results deduced in Sec. II to the midrapidity region of  $p$ - $p$ ,  $p$ -Pb, and Pb-Pb collisions at the LHC to study the behavior of  $B_A$  as a function of the collision system size and the transverse momentum of light nuclei. First we present results of  $B_2$  and  $B_3$  as a function of the effective radius of the hadronic system  $R_f$ . Then we give results of  $B_2$  and  $B_3$  as a function of the charged particle pseudorapidity density  $dN_{ch}/d\eta$ . Finally, we show results of  $B_2$  and  $B_3$  as a function of the transverse momentum per nucleon,  $p_T/A$ .

#### A. $B_A$ as a function of $R_f$

With Eqs. (45) and (46), we calculate  $B_2$  of  $d$  and  $B_3$  of  ${}^3\text{He}$  at the fixed value of  $p_T/A = 0.75$  GeV/ $c$  as a function of the collision system size denoted by  $R_f$ . The results are presented with the solid line and the dash-dotted line in Fig. 1(a) and 1(b), respectively, which show that both  $B_2$  and  $B_3$  decrease with the increase of  $R_f$ , and  $B_3$  decreases more rapidly than  $B_2$ .

In the large- $R_f$  region where  $R_f \gg \sigma_{d/{}^3\text{He}}$ , Eqs. (45) and (46) give

$$B_2 \propto R_f^{-3} \propto V_f^{-1}, \quad (47)$$

$$B_3 \propto R_f^{-6} \propto V_f^{-2}. \quad (48)$$

$V_f$  is the effective volume of the collision system at the freeze-out of light nuclei. These results are consistent with those in Refs. [53,54]. From Eqs. (47) and (48) one can see  $\sqrt{B_3}$  should have a similar behavior as that of  $B_2$  as a function of

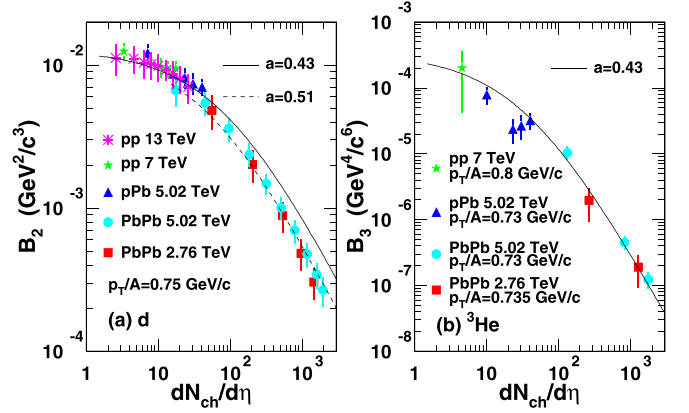


FIG. 2. (a)  $B_2$  of  $d$  and (b)  $B_3$  of  ${}^3\text{He}$  as a function of  $dN_{ch}/d\eta$  in  $p$ - $p$ ,  $p$ -Pb, and Pb-Pb collisions at the LHC. Filled symbols are the data [46,48–51,62], and different lines are our results.

$R_f$ . We plot the result of  $\sqrt{B_3}$  with the dashed line in Fig. 1(a) and find it is indeed almost parallel to  $B_2$  in the large- $R_f$  region such as  $R_f > 4$  fm. But in the small- $R_f$  area,  $\sqrt{B_3}$  is different from  $B_2$  because in this area they are affected by not only  $R_f$  but also  $\sigma_{d/{}^3\text{He}}$  related with different sizes of  $d$  and  ${}^3\text{He}$  themselves.

#### B. $B_A$ as a function of $dN_{ch}/d\eta$

The pseudorapidity density of the charged particles,  $dN_{ch}/d\eta$ , is the most direct observable to represent the size of the collision system. In this section, we study  $B_2$  of  $d$  and  $B_3$  of  ${}^3\text{He}$  as a function of  $dN_{ch}/d\eta$ . To compare with the experimental data, we choose  $p_T/A = 0.75$  GeV/ $c$  for  $d$  and  $p_T/A = 0.735$  GeV/ $c$  for  ${}^3\text{He}$ . The relationship between  $dN_{ch}/d\eta$  and  $R_f$  can be parametrized based on the Hanbury Brown–Twiss (HBT) interferometry as  $R_f = a(dN_{ch}/d\eta)^{1/3}$  [60]. Here the proportionality coefficient  $a$  is a free parameter, and it is located in the range 0.4–1.0 extracted from the HBT correlations in Ref. [61]. We first adopt  $a = 0.43$  to compute  $B_2$  and  $B_3$ . The solid lines in Fig. 2 are our results, and filled symbols are the experimental data [46,48–51,62]. Overall, our results agree with the data of  $B_2$  and  $B_3$  in different collision systems at LHC energies except for overestimations of  $B_2$  in Pb-Pb collisions.

We retune  $a$  to be 0.51 to recompute  $B_2$  in Pb-Pb collisions, and the result presented by the dashed line in Fig. 2(a) reproduces the data very well. In our model, different values of  $a$  means different  $R_f$  at a given  $dN_{ch}/d\eta$  and further means a different freeze-out time. The values 0.51 for  $d$  and 0.43 for  $a$  for  ${}^3\text{He}$  mean that the effective radius of the system at  $d$  freeze-out is about 20% larger than that at  ${}^3\text{He}$  freeze-out. This could either be related to the simplifying assumptions of our model or it might indicate a later freeze-out for  $d$  compared with  ${}^3\text{He}$  in Pb-Pb collisions. We note that this is consistent with the work of the Blast-wave model where it gives that the kinetic freeze-out temperature (transverse expansion velocity) of  $d$  is lower (larger) than that of  ${}^3\text{He}$  [46]. Richer measurements for  ${}^3\text{He}$  are expected to make precise conclusions.

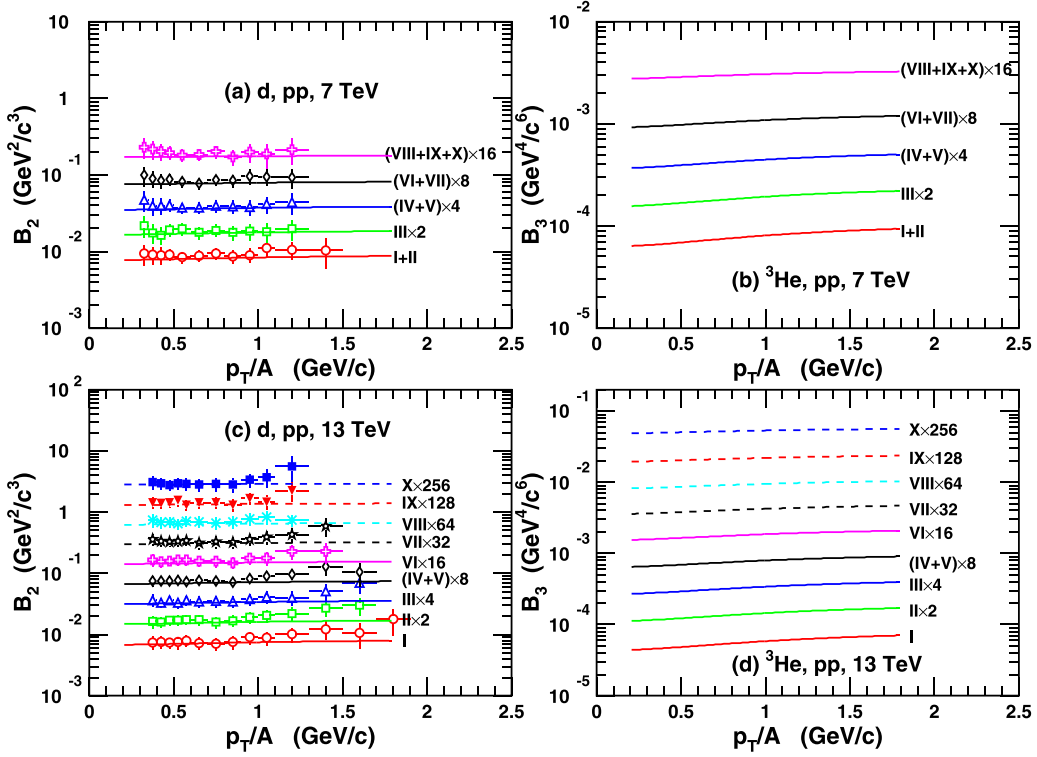


FIG. 3. (a)  $B_2$  of deuterons and (b)  $B_3$  of  ${}^3\text{He}$  as functions of  $p_T/A$  in  $p$ - $p$  collisions at  $\sqrt{s} = 7$  TeV. (c)  $B_2$  of deuterons and (d)  $B_3$  of  ${}^3\text{He}$  as functions of  $p_T/A$  in  $p$ - $p$  collisions at  $\sqrt{s} = 13$  TeV. Symbols are the data from Refs. [50,51], and the different lines are our results.  $B_2$  and  $B_3$  have been scaled by the indicated factors for better visibility.

### C. $B_A$ as a function of transverse momentum

In this section we study the transverse momentum dependence of  $B_A$  in the midrapidity regions in  $p$ - $p$ ,  $p$ -Pb, and Pb-Pb collisions at the LHC. Recalling Eqs. (45) and (46) and considering  $\gamma = (1 + p_T^2/m_d^2)^{1/2}$  at midrapidity, we have

$$B_2(p_T) = \frac{32(\sqrt{\pi}\hbar c)^3 g_d \sqrt{1 + \frac{p_T^2}{m_d^2}}}{m_d (C R_f^2 + \sigma_d^2) \sqrt{C R_f^2 + (1 + \frac{p_T^2}{m_d^2}) \sigma_d^2}}, \quad (49)$$

$$B_3(p_T) = \frac{192\sqrt{3}(\pi\hbar^2 c^2)^3 g^3_{\text{He}} (1 + \frac{p_T^2}{m_{\text{He}}^2})}{m_{\text{He}}^2 (\frac{C}{2} R_f^2 + \sigma_{\text{He}}^2) \sqrt{\frac{C}{2} R_f^2 + (1 + \frac{p_T^2}{m_{\text{He}}^2}) \sigma_{\text{He}}^2}} \times \frac{1}{(\frac{2C}{3} R_f^2 + \sigma_{\text{He}}^2) \sqrt{\frac{2C}{3} R_f^2 + (1 + \frac{p_T^2}{m_{\text{He}}^2}) \sigma_{\text{He}}^2}}. \quad (50)$$

The above two equations show that  $B_2$  and  $B_3$  have close relations with the  $p_T$  of light nuclei.

In particular, if  $R_f$  is much larger than the sizes of light nuclei, such as in central Pb-Pb collisions at the LHC, we have

$$B_2(p_T) = \frac{32(\sqrt{\pi}\hbar c)^3 g_d}{m_d C^{3/2} R_f^3} \sqrt{1 + \frac{p_T^2}{m_d^2}}, \quad (51)$$

$$B_3(p_T) = \frac{1728(\pi\hbar^2 c^2)^3 g^3_{\text{He}}}{m_{\text{He}}^2 C^3 R_f^6} \left(1 + \frac{p_T^2}{m_{\text{He}}^2}\right). \quad (52)$$

Equations (51) and (52) show that both  $B_2$  and  $B_3$  should increase with  $p_T$ , and such an increasing trend of  $B_3$  is stronger than that of  $B_2$ . Otherwise, in the limiting case that  $R_f$  is much smaller than the sizes of light nuclei, we have

$$B_2(p_T) = \frac{32(\sqrt{\pi}\hbar c)^3 g_d}{m_d \sigma_d^3}, \quad (53)$$

$$B_3(p_T) = \frac{192\sqrt{3}(\pi\hbar^2 c^2)^3 g^3_{\text{He}}}{m_{\text{He}}^2 \sigma_{\text{He}}^6}. \quad (54)$$

In this limiting case,  $B_2$  and  $B_3$  are independent of  $p_T$ . From the above discussions, one can see that the  $p_T$  dependence of  $B_A$  is different in different collisions. Such interesting behavior of  $B_A$  as a function of  $p_T$  in different collision systems is a natural characteristic of our model. It can be used to test the validity of our model and the production mechanisms of light nuclei. Next we test it in  $p$ - $p$ ,  $p$ -Pb, and Pb-Pb collisions in LHC experiments.

We first study  $B_2$  and  $B_3$  as functions of  $p_T/A$  in  $p$ - $p$  collisions at  $\sqrt{s} = 7$  TeV and 13 TeV. The results are in Fig. 3. We use the data of  $dN_{ch}/d\eta$  from Refs. [63,64] to determine  $R_f$  by  $R_f = a(dN_{ch}/d\eta)^{1/3}$  and adopting  $a = 0.43$ . Symbols are the data from Refs. [50,51], and different lines are our results.  $B_2$  and  $B_3$  have been scaled with the indicated factors for better visibility. From Fig. 3, one can see that  $B_2$  exhibits nearly

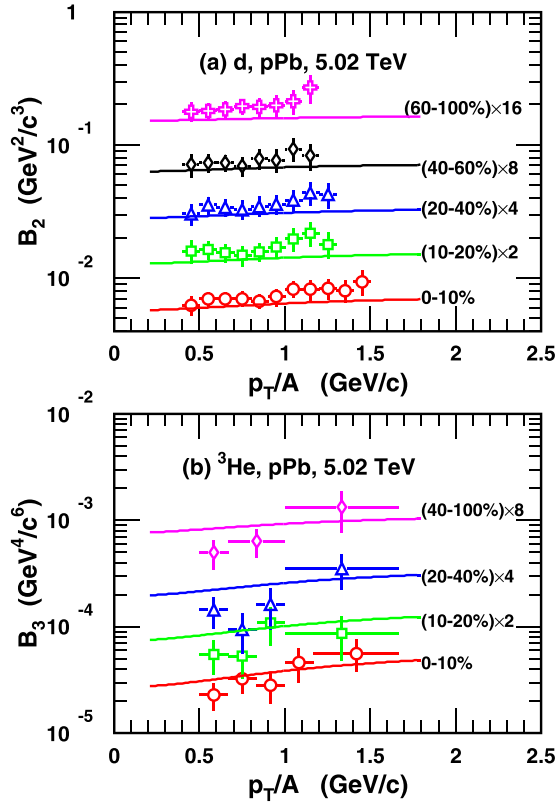


FIG. 4. (a)  $B_2$  of deuterons and (b)  $B_3$  of  ${}^3\text{He}$  as functions of  $p_T/A$  in  $p$ -Pb collisions at  $\sqrt{s_{NN}} = 5.02$  TeV. Open symbols are the data [48,49], and different lines are our results.  $B_2$  and  $B_3$  have been scaled with the indicated factors for better visibility.

constant trends within error bars and  $B_3$  shows very weak  $p_T$  dependence. This is the natural result of Eqs. (49) and (50). In small  $p$ - $p$  collisions,  $R_f$  is even smaller than the sizes of the light nuclei themselves denoted by  $\sigma_d$  or  $\sigma_{{}^3\text{He}}$ . In this case, the item containing  $1 + \frac{p_T^2}{m_{d/{}^3\text{He}}^2}$  in the denominator becomes prominent and can nearly offset the  $p_T$  dependence in the numerator. In the limiting case of  $R_f = 0$  fm, the  $p_T$  dependence in the denominator can completely offset the  $p_T$  dependence in the numerator, and  $B_A$  exhibits constant behavior as the function of  $p_T/A$ . So the smaller of the collision system, the weaker  $p_T$  dependence of  $B_A$  due to the non-negligible size of the light nuclei.

We then study  $B_2$  and  $B_3$  as functions of  $p_T/A$  in  $p$ -Pb collisions at  $\sqrt{s_{NN}} = 5.02$  TeV. The results are in Fig. 4. We use the data of  $dN_{ch}/d\eta$  in Ref. [65] to determine  $R_f$ . Here  $a$  is 0.43, the same as in  $p$ - $p$  collisions. Open symbols are the data [48,49], and the different lines are our results.  $B_2$  and  $B_3$  have been scaled with the indicated factors for better visibility. From Fig. 4, one can see that our results can reproduce the behavior of  $B_2$  and  $B_3$  measured experimentally. In  $p$ -Pb collisions,  $R_f$  becomes comparable to the sizes of the light nuclei themselves. So  $B_2$  and  $B_3$  begin to increase as a function of  $p_T$ .

We finally calculate  $B_2$  and  $B_3$  as functions of  $p_T/A$  in Pb-Pb collisions at  $\sqrt{s_{NN}} = 2.76$  TeV and 5.02 TeV. We use

the data of  $dN_{ch}/d\eta$  in Refs. [66,67] to determine  $R_f$ .  $a$  is 0.43 for  ${}^3\text{He}$ , the same as in  $p$ - $p$  and  $p$ -Pb collisions, while it is 0.51 for  $d$ . Symbols with error bars in Fig. 5 are the data [46,47,62], and the different lines are our theoretical results. From Fig. 5, one can see that the rising behavior of the data can be described by our results and this rising trend becomes stronger from peripheral to central collisions. This rising trend as a function of the transverse momentum can be naturally explained in our model by setting nucleon coalescence criteria in the rest frame of the nucleon pair (three-nucleon cluster) rather than in the laboratory frame. Recalling that  $B_A$  presents the probability of nucleons combining into light nuclei, when transformed from the laboratory frame to the nucleon-pair rest frame, the coordinate space which the nucleons are in, is Lorentz contracted. So their relative distance becomes smaller and it becomes easier for them to coalesce into light nuclei. The larger transverse momentum means larger velocity and also means stronger contraction. This leads to larger coalescence probability.

At the end of this section, we want to point out that  $R_f$  is parametrized to be  $p_T$  independent to give numerical results in this paper. From the latest experimental measurements for femtoscopic correlations of particle pairs [two pions, two kaons, and two (anti)protons], one sees that  $R_f$  exhibits a decreasing trend as a function of  $p_T$  [68]. Our equations (49) and (50) clearly show that  $B_2$  and  $B_3$  would increase stronger if  $R_f$  decreases as a function of  $p_T$ , especially in central heavy-ion collisions. This would improve our numerical results in Pb-Pb collisions in Fig. 5. But due to very limited  $p_T$  range and large error bars of  $R_f$  obtained from two (anti)proton correlation measurements, it is hard to quantitatively study effects on  $B_A$  factors resulting from the  $p_T$  dependence of  $R_f$  currently.

#### IV. SUMMARY

Inspired by the interesting behavior of the coalescence factors  $B_A$  of light nuclei measured experimentally, we studied the momentum dependence of the production of deuterons and helions in high-energy collisions in the framework of nucleon coalescence. We derived the momentum spectra for  $d$  and  ${}^3\text{He}$ . To get intuitionistic expressions for the momentum dependence of light nuclei, in particular, those for  $B_A$  factors, we took a few assumptions and/or approximations such as the factorization of coordinate and momentum dependencies of the kernel functions and the normalized joint nucleon distributions. We obtained simple formulas of the momentum spectra of  $d$  and  ${}^3\text{He}$ , and, in particular, we gave analytic expressions for momentum-dependent  $B_A$  and discussed their properties as functions of the collision system size as well as the light nuclei size and momentum.

We applied the results deduced to the midrapidity regions of  $p$ - $p$ ,  $p$ -Pb, and Pb-Pb collisions at the LHC. We reproduced the rapidly decreasing behavior of the data of  $B_2$  and  $B_3$  as a function of  $dN_{ch}/d\eta$ . In central and semicentral Pb-Pb collisions at  $dN_{ch}/d\eta > 100$ , we found that the effective radius of the system at  $d$  freeze-out was about 20% larger than that at  ${}^3\text{He}$  freeze-out. Since the larger radius usually means the later time during system expansion evolution, our results might indicate later freeze-out for  $d$  compared with  ${}^3\text{He}$  in Pb-Pb

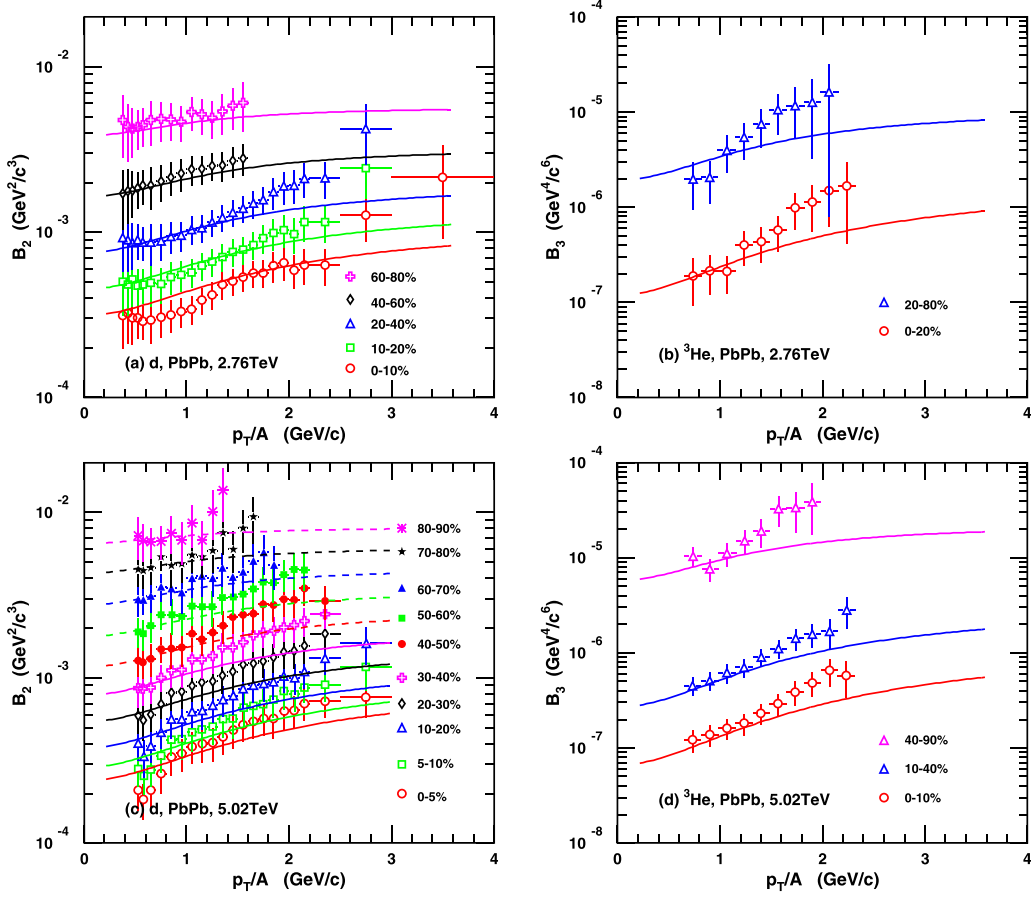


FIG. 5. (a)  $B_2$  of deuterons and (b)  $B_3$  of  ${}^3\text{He}$  as functions of  $p_T/A$  in Pb-Pb collisions at  $\sqrt{s_{NN}} = 2.76$  TeV. (c)  $B_2$  of deuterons and (d)  $B_3$  of  ${}^3\text{He}$  as functions of  $p_T/A$  in Pb-Pb collisions at  $\sqrt{s_{NN}} = 5.02$  TeV. Symbols with error bars are the data [46,47,62] and the different lines are our results at different centralities.

collisions. Furthermore, we gave natural explanations for the obvious growth of  $B_A$  against  $p_T$  for all centralities in Pb-Pb collisions and relatively weak  $p_T$  dependencies of  $B_A$  in  $p$ - $p$  and  $p$ -Pb collisions at the LHC.

At last, we want to discuss that the present paper focuses on common features of the coalescence mechanism in describing the production of light nuclei in different collision systems, and the dynamical details in the coalescence process are not included. We try our best to intuitively present effects of kernel functions in the rest frame of the nucleon cluster and their interesting influences on  $B_A$  at different  $p_T$  bins in  $p$ - $p$ ,  $p$ -Pb, and Pb-Pb collisions. We have taken the coordinate and momentum factorization assumption which means that the flow effect is ignored. The flow in different collision systems is very different, and its effect on light nuclei

production, especially in relativistic heavy-ion collisions, is another interesting issue and deserves to be further considered carefully.

#### ACKNOWLEDGMENTS

We thank Xiao-Feng Luo and Lie-Wen Chen for helpful discussions. This work was supported in part by the National Natural Science Foundation of China under Grant No. 11975011, the Natural Science Foundation of Shandong Province, China, under Grants No. ZR2020MA097, No. ZR2019YQ06, and No. ZR2019MA053, and the Higher Educational Youth Innovation Science and Technology Program of Shandong Province under Grants No. 2020KJJ004 and No. 2019KJJ010.

- [1] R. Hagedorn, *Phys. Rev. Lett.* **5**, 276 (1960).
- [2] S. T. Butler and C. A. Pearson, *Phys. Rev. Lett.* **7**, 69 (1961).
- [3] H. H. Gutbrod *et al.*, *Phys. Rev. Lett.* **37**, 667 (1976).
- [4] S. Zhang, J. H. Chen, H. Crawford, D. Keane, Y. G. Ma, and Z. B. Xu, *Phys. Lett. B* **684**, 224 (2010).

- [5] A. Bzdak, S. Esumi, V. Koch, J. Liao, M. Stephanov, and N. Xu, *Phys. Rep.* **853**, 1 (2020).
- [6] K. J. Sun, L. W. Chen, C. M. Ko, J. Pu, and Z. B. Xu, *Phys. Lett. B* **781**, 499 (2018).
- [7] Z. Citron *et al.*, *CERN Yellow Rep. Monogr.* **7**, 1159 (2019).

- [8] P. Junnarkar and N. Mathur, *Phys. Rev. Lett.* **123**, 162003 (2019).
- [9] P. Braun-Munzinger and B. Dönigus, *Nucl. Phys. A* **987**, 144 (2019).
- [10] D. Oliinychenko, *Nucl. Phys. A* **1005**, 121754 (2021).
- [11] S. T. Butler and C. A. Pearson, *Phys. Rev.* **129**, 836 (1963).
- [12] A. Schwarzschild and C. Zupancic, *Phys. Rev.* **129**, 854 (1963).
- [13] H. Sato and K. Yazaki, *Phys. Lett. B* **98**, 153 (1981).
- [14] C. B. Dover, U. Heinz, E. Schnedermann, and J. Zimányi, *Phys. Rev. C* **44**, 1636 (1991).
- [15] R. Mattiello, A. Jahns, H. Sorge, H. Stöcker, and W. Greiner, *Phys. Rev. Lett.* **74**, 2180 (1995).
- [16] J. L. Nagle, B. S. Kumar, D. Kusnezov, H. Sorge, and R. Mattiello, *Phys. Rev. C* **53**, 367 (1996).
- [17] R. Mattiello, H. Sorge, H. Stöcker, and W. Greiner, *Phys. Rev. C* **55**, 1443 (1997).
- [18] L.-W. Chen, C. M. Ko, and B.-A. Li, *Phys. Rev. C* **68**, 017601 (2003).
- [19] W. Zhao, L. Zhu, H. Zheng, C. M. Ko, and H. Song, *Phys. Rev. C* **98**, 054905 (2018).
- [20] J. L. Nagle, B. S. Kumar, M. J. Bennett, G. E. Diebold, J. K. Pope, H. Sorge, and J. P. Sullivan, *Phys. Rev. Lett.* **73**, 1219 (1994).
- [21] A. Polleri, J. P. Bondorf, and I. N. Mishustin, *Phys. Lett. B* **419**, 19 (1998).
- [22] R. Scheibl and U. Heinz, *Phys. Rev. C* **59**, 1585 (1999).
- [23] N. Sharma, T. Perez, A. Castro, L. Kumar, and C. Nattrass, *Phys. Rev. C* **98**, 014914 (2018).
- [24] S. Bazak and S. Mrówczyński, *Mod. Phys. Lett. A* **33**, 1850142 (2018).
- [25] K. Blum and M. Takimoto, *Phys. Rev. C* **99**, 044913 (2019).
- [26] A. Mekjian, *Phys. Rev. Lett.* **38**, 640 (1977).
- [27] P. J. Siemens and J. I. Kapusta, *Phys. Rev. Lett.* **43**, 1486 (1979).
- [28] A. Andronic, P. Braun-Munzinger, J. Stachel, and H. Stöcker, *Phys. Lett. B* **697**, 203 (2011).
- [29] J. Cleymans, S. Kabana, I. Kraus, H. Oeschler, K. Redlich, and N. Sharma, *Phys. Rev. C* **84**, 054916 (2011).
- [30] A. Andronic, P. Braun-Munzinger, K. Redlich, and J. Stachel, *Nature (London)* **561**, 321 (2018).
- [31] Y. Cai, T. D. Cohen, B. A. Gelman, and Y. Yamauchi, *Phys. Rev. C* **100**, 024911 (2019).
- [32] P. Danielewicz and G. F. Bertsch, *Nucl. Phys. A* **533**, 712 (1991).
- [33] S. Sombun, K. Tomuang, A. Limphirat, P. Hillmann, C. Herold, J. Steinheimer, Y. Yan, and M. Bleicher, *Phys. Rev. C* **99**, 014901 (2019).
- [34] D. Oliinychenko, L.-G. Pang, H. Elfner, and V. Koch, *Phys. Rev. C* **99**, 044907 (2019).
- [35] Y. Oh, Z.-W. Lin, and C. M. Ko, *Phys. Rev. C* **80**, 064902 (2009).
- [36] D. Oliinychenko, L.-G. Pang, H. Elfner, and V. Koch, *MDPI Proc.* **10**, 6 (2019).
- [37] S. Afanasiev *et al.* (PHENIX Collaboration), *Phys. Rev. Lett.* **99**, 052301 (2007).
- [38] L. Adamczyk *et al.* (STAR Collaboration), *Phys. Rev. C* **94**, 034908 (2016).
- [39] L. Adam *et al.* (STAR Collaboration), *Phys. Rev. C* **102**, 044906 (2020).
- [40] D. Zhang (for the STAR Collaboration), *Nucl. Phys. A* **1005**, 121825 (2021).
- [41] C. Adler *et al.* (STAR Collaboration), *Phys. Rev. Lett.* **87**, 262301 (2001).
- [42] J. Adam *et al.* (STAR Collaboration), *Phys. Rev. C* **99**, 064905 (2019).
- [43] S. Acharya *et al.* (ALICE Collaboration), *Phys. Rev. C* **102**, 055203 (2020).
- [44] S. Acharya *et al.* (ALICE Collaboration), *Phys. Lett. B* **805**, 135414 (2020).
- [45] M. Colocci (for the ALICE Collaboration), *Nucl. Phys. A* **982**, 895 (2019).
- [46] J. Adam *et al.* (ALICE Collaboration), *Phys. Rev. C* **93**, 024917 (2016).
- [47] S. Acharya *et al.* (ALICE Collaboration), *Eur. Phys. J. C* **77**, 658 (2017).
- [48] S. Acharya *et al.* (ALICE Collaboration), *Phys. Lett. B* **800**, 135043 (2020).
- [49] S. Acharya *et al.* (ALICE Collaboration), *Phys. Rev. C* **101**, 044906 (2020).
- [50] S. Acharya *et al.* (ALICE Collaboration), *Phys. Lett. B* **794**, 50 (2019).
- [51] S. Acharya *et al.* (ALICE Collaboration), *Eur. Phys. J. C* **80**, 889 (2020).
- [52] J. Chen, D. Keane, Y.-G. Ma, A. Tang, and Z. Xu, *Phys. Rep.* **760**, 1 (2018).
- [53] F. Bellini and A. P. Kalweit, *Phys. Rev. C* **99**, 054905 (2019).
- [54] F. Bellini and A. P. Kalweit, *Acta Phys. Pol., B* **50**, 991 (2019).
- [55] R. Q. Wang, J. Song, G. Li, and F. L. Shao, *Chin. Phys. C* **43**, 024101 (2019).
- [56] L. W. Chen, C. M. Ko, and B. A. Li, *Nucl. Phys. A* **729**, 809 (2003).
- [57] L. Zhu, C. M. Ko, and X. Yin, *Phys. Rev. C* **92**, 064911 (2015).
- [58] S. Mrówczyński, *Acta Phys. Pol., B* **48**, 707 (2017).
- [59] I. Angeli and K. P. Marinova, *At. Data Nucl. Data Tables* **99**, 69 (2013).
- [60] M. A. Lisa, S. Pratt, R. Soltz, and U. Wiedemann, *Annu. Rev. Nucl. Part. Sci.* **55**, 357 (2005).
- [61] J. Adam *et al.* (ALICE Collaboration), *Phys. Rev. C* **93**, 024905 (2016).
- [62] M. Puccio, Ph.D. thesis, Turin University, 2017, <http://cds.cern.ch/record/2309824>.
- [63] J. Adam *et al.* (ALICE Collaboration), *Nat. Phys.* **13**, 535 (2017).
- [64] S. Acharya *et al.* (ALICE Collaboration), *Eur. Phys. J. C* **80**, 167 (2020).
- [65] B. Abelev *et al.* (ALICE Collaboration), *Phys. Lett. B* **728**, 25 (2014).
- [66] B. Abelev *et al.* (ALICE Collaboration), *Phys. Rev. C* **88**, 044910 (2013).
- [67] S. Acharya *et al.* (ALICE Collaboration), *Phys. Rev. C* **101**, 044907 (2020).
- [68] J. Adam *et al.* (ALICE Collaboration), *Phys. Rev. C* **92**, 054908 (2015).